Laser Terahertz Emission Microscope

M. Tonouchi, N. Uchida, S. Kim, R. Inoue, and H. Murakami
Institute of Laser Engineering, Osaka University
2-6 Yamadaoka, Suita, Osaka 565-0871, Japan
Email: tonouchi@ile.osaka-u.ac.jp

Abstract: Laser terahertz (THz) emission microscope (LTEM) is reviewed. Femtosecond lasers can excite the THz waves in various electronic materials due to ultrafast current modulation. The current modulation is realized by acceleration or deceleration of photo-excited carriers, and thus LTEM visualizes dynamic photo-response of substances. We construct free-space type and scanning probe one with transmission or reflection modes. The developed systems have a minimum spatial resolution better than 2 μm, which is defined by the laser beam diameter. We also present some examples of LTEM applications.

Keywords: Terahertz radiation, Microscope, High resolution active imaging

doi: 10.11906/TST.028-036.2008.03.04

I. Introduction

One can observe terahertz (THz) radiation from various kinds of materials such as semiconductors, high-Tc superconductors (HTSC), colossal magnetoresistance manganites, and multiferroic materials, when excited with a femtosecond laser, owing to ultrafast current modulation [1]. THz waves reflect various kinds of properties such as local electric field, particularly ultrafast transient phenomena, in their waveforms. The observation of the THz waveforms enables us to explore ultrafast nature of electronic materials and devices as a THz emission spectroscopy.

When one excites the THz emission from a certain substance with the femtosecond optical pulses and visualizes the emission image by scanning the laser beam on it, the resolution of the image is limited by the laser beam diameter rather than THz wavelength. Thus construction of a laser-THz emission microscope (LTEM) [2] would provide a new tool for material science and application. We have proposed such LTEM and applied to various materials and devices.

This paper reviews the recent progress of the LTEM development and its applications. The LTEM system originated from the two-dimensional scan of THz emission on the photoconductive antenna for developing an effective emitter. Thus, when it is applied to superconductors, it can visualize the supercurrent distribution because the amplitude of the THz radiation from the superconductor is proportional to the supercurrent density [3,4]. We also put forward it to visualize ferroelectric domain in mautiferroic material, $BiFeO_3$ [5,6]. Recently, as a unique application, it demonstrated a new possibility for inspecting electrical faults in semiconductor integrated circuits [7]. Consequently, it is a valuable tool not only for basic science but also for industrial applications.

II. Experimental

The basic LTEM system is illustrated schematically in Fig. 1. A mode-locked Ti:sapphire laser that produces femtosecond optical pulses with a pulse-width of 100 fs is used as the optical source. The center wavelength of the pulses is about 790 nm and the repetition rate is 82 MHz. The excitation pulses are split from the trigger pulses using a beam splitter and focused with an optical lens onto a sample such as an IC chip mounted on a

computer-controlled x-y stage. The THz waves are collimated and focused onto a detector using a pair of off-axis parabolic mirrors. We use a bow-tie type photoconductive antenna as the detector. One of the parabolic mirrors has a hole with a diameter of 3 mm, through which the pump pulses are introduced to the sample. The detector is gated using trigger pulses. The amplitude of the THz emissions is mo-nitored using a lock-in amplifier. The THz emission images are constructed by mapping the amplitude. Details of the LTEM system have been reported elsewhere [4].

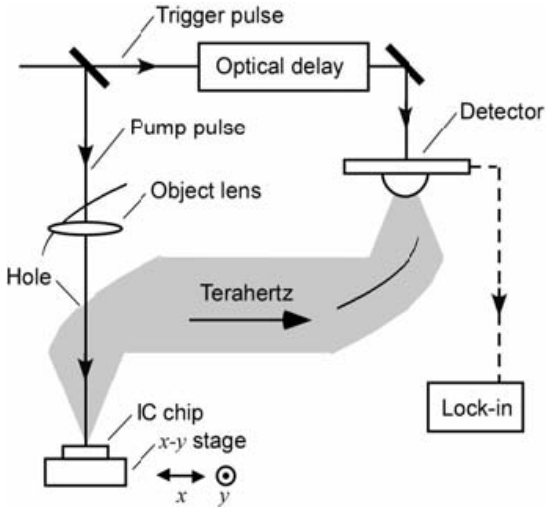

Fig. 1 Schematic diagram of the back-scattered-type LTEM system. THz waves are transmitted in the gray region.

One can construct various kinds of configurations. In the prototype LTEM [7], a spatial resolution was about 20 μm because a parabolic mirror with a hole between objective lens and sample was used, as shown in Fig. 2(a). For better resolution, the indium tin oxide (ITO)-coated glass instead of the parabolic mirror with a hole was used in order to focus the laser pulse and collect the backward THz emission (Fig. 2(b)) [8]. As a result, the spatial resolution improved up to about 3 μm. Also a similar configuration with Fig. 2(b) was tried using ITO-coated glass and objective lens for better focusing of laser beam as shown in Fig. 2(c) [9]. It is almost transparent for the visible light and highly reflective for the THz waves. By introducing it between a sample and a focusing optics, we can reduce the distance between the sample and the focusing optics, and decrease the beam diameter at the front side of a sample. The release of these limitations allows us to adopt a suitable focusing optics with a high NA value.

Same resolution was achieved by scanning probe (SP)-LTEM [10] where laser pulse is carried by optical fiber probe and thus the resolution is limited by a diameter of optical fiber (Fig. 2(d)). In addition to the reflection type LTEMs, the transmission type is available for some materials.

Some other techniques are also developed to improve the spatial resolution. One is an introduction of a beam expander in front of objective lens. By expanding the incident beam diameter Φ, we can improve the beam spot size φ, according to the following relation,

$$\phi = \frac{4}{\pi}\lambda\frac{f}{\Phi} \qquad (1)$$

where λ is a wavelength, and *f* is the focal length of the objective lens.

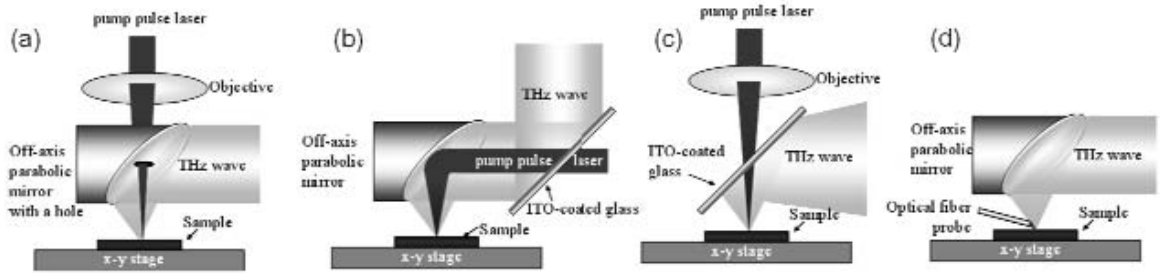

Fig. 2 Various configurations for irradiating a laser and collecting THz wave using (a) the off-axis parabolic mirror with a hole, (b) the off-axis parabolic mirror without hole and the ITO-coated glass, (c) objective lens and ITO-coated glass, (d) optical fiber probe and off-axis parabolic mirror.

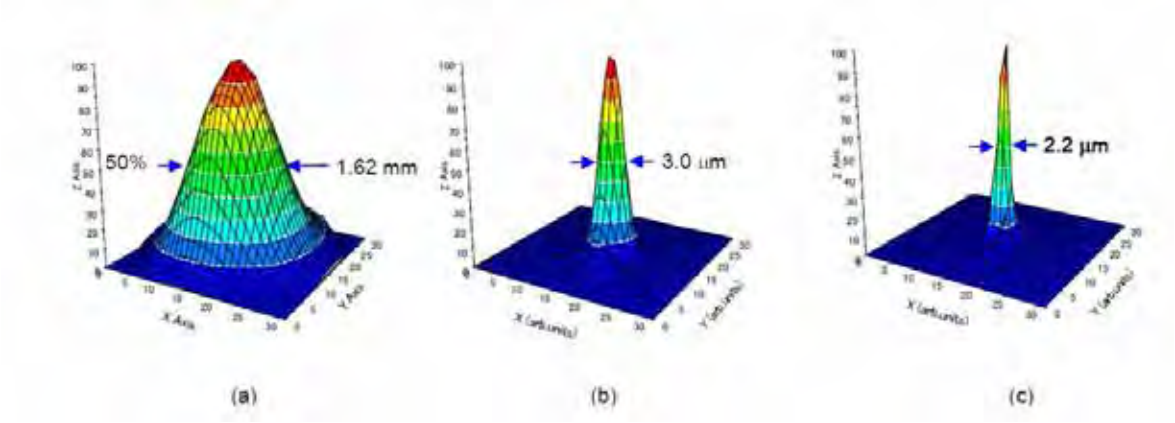

Fig.3 pump beam power profiles observed under several conditions. (a) Beam power profile of laser emitted from the fiber laser, (b)beam power profile of pump beam after passing through an objective lens, and (c) after passing through the objective lens and beam expander with the magnification of 3 times.

Figure 3 shows the beam power profiles observed under several conditions; (a), (b), and (c) show the profiles without any optics, after passing through an objective lens (Mitsutoyo M PLAN APO 20, NA=0.4) without the beam expander, and with it. Comparing these results, introduction of the beam expander has an certain effect on reducing the beam spot size down to about 73% (2.2μmφ). Furthermore, since the beam spot size in the prototype LTEM system was at most about 20 μmφ, it is obviously expected that the introduction of the objective lens is effective to improve the spatial resolution.

Another technique is to use a solid immersion lens (SIL). The full-width at half-maximum (FWHW) spot size *s* is given by $\lambda/(2NA)$ in the scalar approximation, where $NA = n \sin\theta$ is the numerical aperture, θ is the maximum angle of rays in the focused beam, and *n* is the index of refraction at the focus [11]. Thus, the small *s* can be achieved by increasing the effective numerical aperture NA_{eff} of the optical system. For this purpose, we employ SIL on the surface of the sample as illustrated in Fig. 4.

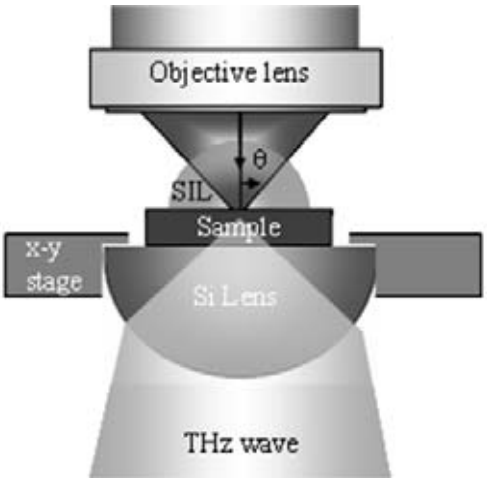

Fig. 4 Schematic diagram of transmission-type LTEM. A solid immersion lens (SIL) is set at the front side of sample, and for effective THz collection, a hemispherical silicon lens is attached to the back side.

To evaluate the spatial resolution, the photoconductive antenna switches with so-called *line and space pattern* (Fig. 5) were fabricated on Fe-doped indium phosphide (InP) substrate by the conventional photolithography method. InP is commonly used for high power THz emitter. Here the width of Au strip lines (W_L) and spaces between them (W_S) were designed to have the same size varying from 1.5 μm to 5 μm. We refer to the sample with W_L=W_S=3 μm as "3 μm sample."

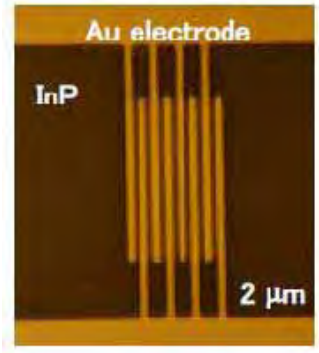

Fig. 5 Gold line and space patterns on Fe-doped semi-insulating InP. The widths of the line and space are 2μm each.

III. LTEM performance

Figure 6 shows the LTEM images of 5 μm sample and its line scan profile of THz emission amplitude along *x*-axis at the applied voltage of V=0.5V and 0V [12]. For better understanding, we superposed LTEM images with the photograph. For imaging, the sample was scanned with a spatial resolution of 0.2 μm for *x*-axis and 1 μm for *y*-axis. The scan area of LTEM is 90(*x*)×5(*y*) μm^2 and the scan time is about 4 min.

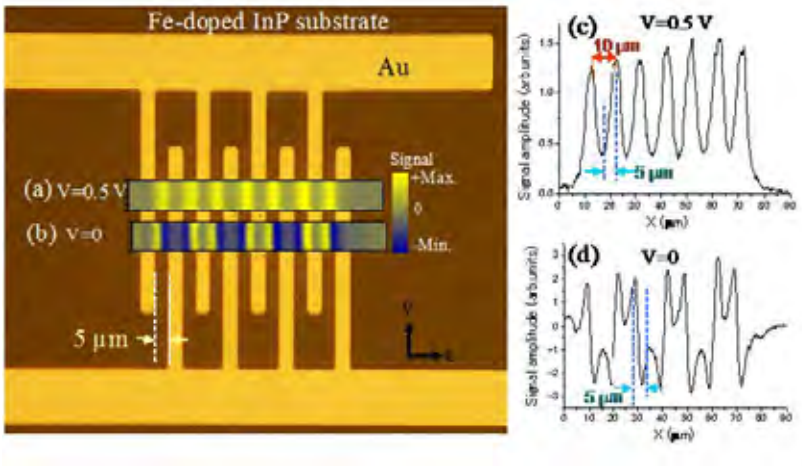

Fig. 6 Photograph of 5 μm sample superposed with LTEM images at (a) the applied voltage V=0.5 V and (b) without bias V=0 V. Each scan area of LTEM images is 90×5 μm^2. Line scan profiles of THz emission amplitude along *x*-axis at (c) V=0.5 V and (b) without bias V=0 V.

From the superposition with the photograph, one can find that signal amplitude corresponding to THz emission appears from the gaps (spaces) between electrodes. Shown in Fig. 6(c), the 7 maxima of signal correspond to the space number between 8 electrodes. Here, note that only positive signal was observed at V=0.5 V. This originated the fact that the transient current generated by fs laser will flow along Au electrodes including long horizontal lines. and the detector can only detect a horizontal polarization component. In the case of zero bias condition, only the photo-excited carriers near the boundary regions between Au electrodes and InP substrate can generate the transient photo current, which is accelerated by the built-in field and is injected into the gold electrodes. As a result, polarization of the radiation field is opposite along neighboring electrodes that are connected to upper and lower horizontal electrodes alternately. Also, these positive and negative responses can be understood by the transient photocurrent flow induced by built-in field and antenna effect.

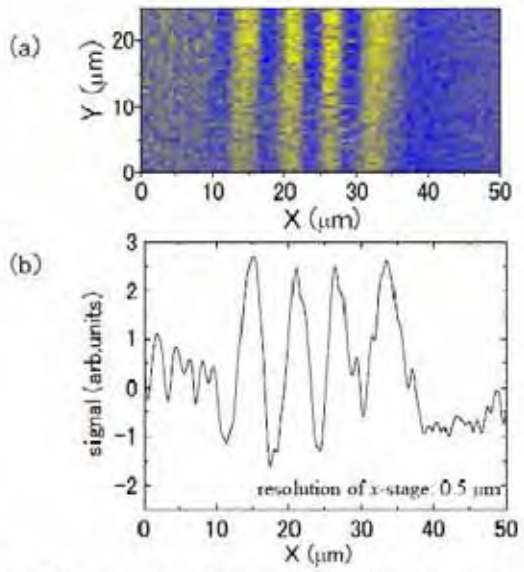

Fig.7 (a) A LTEM image and (b) a line scan profile observed on the 1.5 μm-line and space patterns at a zero bias voltage condition. The observations were carried out by introduction of the beam expander. The resolution of x-y stages are 0.5 μm.

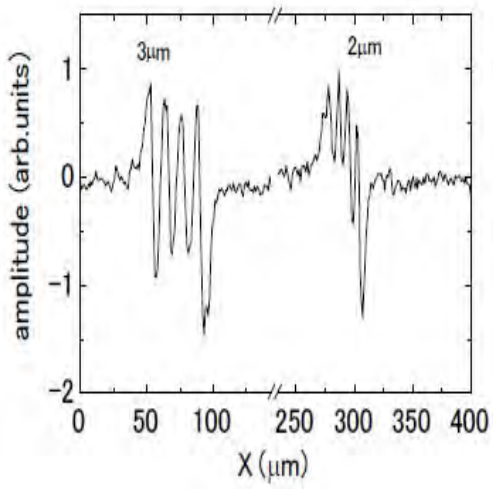

Fig. 8 A line scan profile observed on the 3&2μm-line and space patterns at zero bias voltage condition.

Figure 8 shows a THz wave emission image (upper one) and line scan profile (lower one) observed at a zero bias voltage condition with the beam expander, and without SIL. Although the image was slightly distorted, the 1.5 μm-line and space image was clearly obtained.

Figure 8 shows an example of the line scan profile of the 3μm and 1.5μm line and space samples obtained by SP-LTEM. This also can visualize the image at a spatial resolution of around 2μm.

IV. LTEM application

The THz waves are generated by means of optical carrier excitation followed by either its acceleration or deceleration due to transient polarization. In general the emission properties are governed by the nature of materials such as carrier mobility, mechanism of conductivity and/or photoexcitation, local built-in electric field, and ferroelectricity as well as external contribution such as bias field. Thus LTEM could be a strong research tool for material science. As one of such applications, we show an example of ferroelectric domain imaging.

Typical ferroelectric materials have large optical band gap in ultra-violet region, which makes it difficult to generate THz waves via optical carrier excitation with Ti:sapphire laser at around a wavelength of 780nm. Here we select $BiFeO_3$ to examine, which has relatively small energy gap of about 2.5 eV. $BiFeO_3$ is a multiferroic material displaying ferroelectricity below 1100 K and antiferromagnetism below 640 K, which, in addition, exhibits an extremely large spontaneous polarization *P*s in thin film form providing its potential as a capacitor in various electronic devices. Accordingly, studies on $BiFeO_3$ have mainly been focused on developing its electronic functionality as a capacitor, and its optical functionality, on the other hand, has not been investigated intensively so far. The second harmonic of a mode-locked Ti:Sapphire laser is used for carrier excitation in giving rise to THz radiation[5]. 200 nm-thick $BiFeO_3$ thin films are grown on $(LaAlO_3)_{0.3}(Sr_2AlTaO_6)_{0.7}(001)$ substrates by pulsed laser deposition technique with a KrF excimer laser. A dipole-type photoconductive switch with a pair of Au electrodes is designed on the film by a conventional lift-off process and sputtering method. The Au electrode of the photoconductive switch consists of a pair of 30 μm-wide

strip lines separated by 20 μm with a dipole gap of 10μm. Details of the experiments can be found elsewhere [5,6].

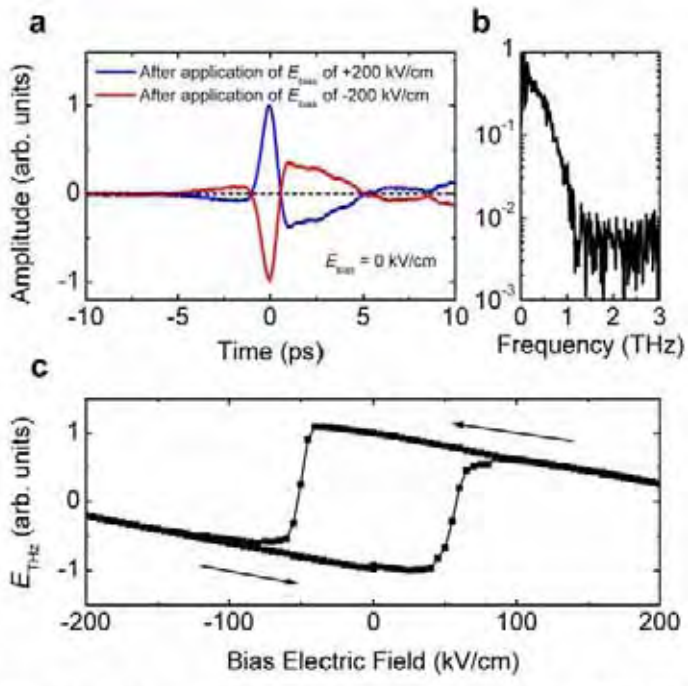

Fig. 9 Terahertz (THz) radiation characteristics of the Bi-FeO_3 thin films**. a,** Time-domain waveforms of the THz pulse radiated from a $BiFeO_3$ film. The measurement was performed at zero-bias electric field once after applying a bias electric field E_{bias} of ±200 kV/cm. The dashed line represents the zero-level line shown for clarity. **b**, Fourier transformed amplitude spectrum of the time-domain wave-forms in **a**. Both waveforms exhibit the same power spectrum since the two waveforms show a similar shape only with their phase shifted by π. **c**, The amplitude of the radiated THz pulse *E*THz as a function of E_{bias}. The arrows indicated the sequential directions starting by applying E_{bias} of +200 kV/cm.

Figure 9(a) shows two time-domain THz waveforms radiated from the $BiFeO_3$ photoconductive switch measured at zero-bias electric field, once after applying a bias electric field E_{bias} of ±200 kV/cm. The THz waveforms show an identical Fourier transformed amplitude spectrum exhibiting a frequency component extending up to 1 THz, (Fig. 9(b)) and obviously, have a reversed phase by *p* with one another. This feature definitely expresses a ferroelectric peculiarity that the history of *E*bias is memorized and the remnant polarization of $BiFeO_3$ substitutes for *E*bias. Further supporting this aspect, a distinct feature was observed as we measured the main peak amplitude of the THz pulse E_{THz} as a function of E_{bias} (Fig. 9(c)). In the photoconductive switches reported so far, which are all non-ferroelectric materials, E_{THz} generally has a linear relationship with the applied E_{bias} reversing its phase by *p* when the polarity of E_{bias} is reversed. However, in the case of $BiFeO_3$, we observed a clear hysteresis loop which looks familiar with the typical polarization hysteresis loop observed in common ferroelectrics. These characteristics strongly indicate the direct relationship of THz radiation with Ps, and implies that the THz radiation here is derived from the ultrafast Ps modulation introduced by the mobile photoexcited charge carriers.

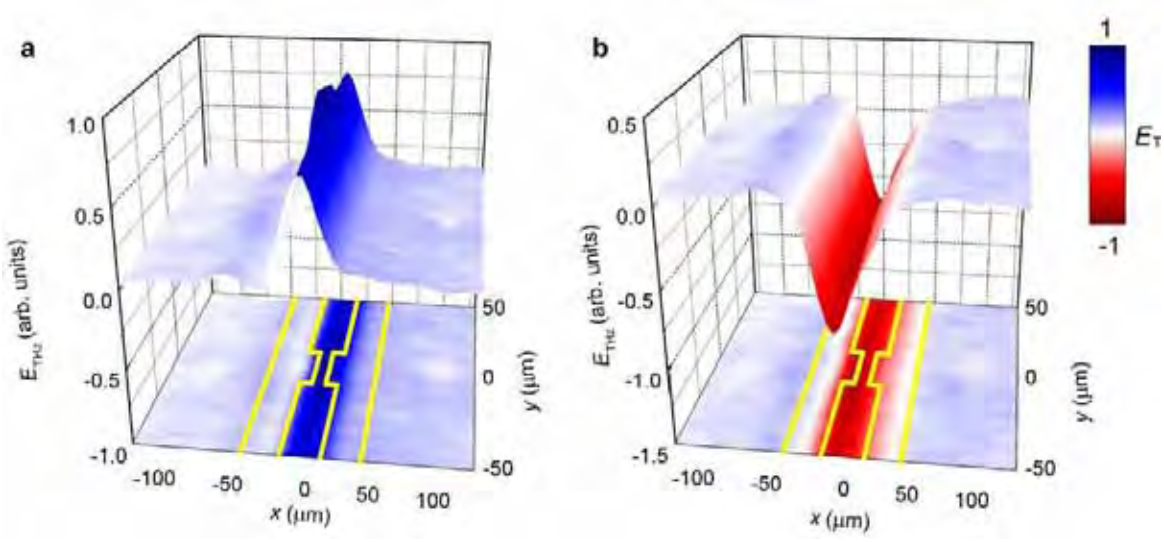

Fig. 10 Visualization of 180˚ ferroelectric domain structure of the $BiFeO_3$ thin film probing with terahertz (THz) radiation. Domain structure under zero-bias voltage measured after applying **a**, +200 V and **b**, −200 V. The geometry of the dipole-type gold electrodes is also shown by the yellow line in the respective images. The spatial resolution here is estimated to be about 20 μm assuming from the diameter of the laser spot.

Since the THz radiation exhibiting direct relationship with the polarization state, LTEM to measure E_{THz} allows us to visualize the ferroelectric domain structures by distinguishing the polarization state from the signs of E_{THz}. In Fig. 10, two kinds of ferroelectric domain images of a section of the $BiFeO_3$ thin film measured at zero-bias voltage after applying a bias voltage V_{bias} of ±200 V. Domains with opposite polarization states appear as blue and red areas depending on the sign of E_{THz}. By comparing the two images, one can see that only the domains between the electrodes has changed their states by the application of opposite V_{bias}, while the other areas are independent of V_{bias} and remain unchanged. Note that we also observed THz radiation even in the areas apart from the electrodes where the domains had not been artificially aligned. However, the intensity of E_{THz} in these areas is relatively weak presumably because the domains are not aligned neatly as it is between the electrodes. These imaging results indicate that THz radiation occurs from individual ferroelectric domains and the intensity of E_{THz} is determined by the average of the electric dipole moments of which the laser spot covers.

LTEM is also applied to visualize for LSI [8], MOS, magnetic flux trapped in HTCSs [4], and so on.

V. Summary

LTEM was proposed and developed. We successfully captured two-dimensional images of THz emission from various kinds of materials and devices. The results suggest that the LTEM system will be a useful tool for scientific imaging, and inspecting LSI chips.

Acknowledgments

This work was supported the Grant-in-Aid for Scientific Research (B) No.19360161.

References

[1] For reviews, see, D. Mittleman, ed., *Sensing with Terahertz Radiation* (Springer, 2003), T. Kobayashi, H. Hirakawa and M. Tonouchi, eds., *Vortex Electronics and SQUIDs*(Springer, 2003), K. Sakai, ed., *Terahertz Optoelectronics* (Springer, 2005)

[2] I. Brener, D. Dykaar, A. Frommer, L. N. Pfeiffer, J. Lopata, J. Wynn, and K. West, and M. C. Nuss, "Terahertz emission from electric field singularities in biased semiconductors," *Opt. Lett.* Vol. 21, pp. 1924–1926, Dec. (1996).

[3] S. Shikii, T. kondo, M. Yamashita, M. Tonouchi, and M. Hangyo, "Observation of supercurrent distribution in $YBa_2Cu_3O_7$ thin films using THz radiation excited with femtosecond laser pulses," *Appl. Phys. Lett.*,Vol.74, pp.1317–1319, Mar. (1999).

[4] M. Tonouchi, M. Yamashita, and M. Hangyo, "Terahertz radiation imaging of supercurrent distribution in vortex-penetrated $YBa_2Cu_3O_{7-\delta}$ thin films strips," *J. Appl. Phys*., Vol.87, pp. 7366–7375, May (2000).

[5] K. Tahakashi, N. Kida, and M. Tonouchi," Terahertz radiation by an ultrafast spontaneous polarization modulation of multiferroic $BiFeO_3$ thin films," *Phys. Rev. Lett*. Vol 96, No.11, 117402, Mar. (2006).

[6] D. S. Rana, K. Tahakashi, K. R. Mavani, I. Kawayama, H. Murakami, and M. Tonouchi, " Visualization of photoassisted polarization switching and its consequences in $BiFeO_3$ thin films probed by terahertz radiation," *Appl. Phys. Lett.* Vol. 91, No.3, 031909, Jul. (2007).

[7] T. Kiwa, M. Tonouchi, M. Yamashita, and K. Kawase, "Laser terahertz emission microscope for inspecting electrical failures in integrated circuits," *Opt. Lett*., Vol.28, pp.2058–2060, Nov. (2003).

[8] M. Yamashita, K. Kawase, C.Otani, T. Kiwa, and M. Tonouchi, "Imaging of large-scale integrated circuits using laser terahertz emission microscopy," *Opt. Exp*., Vol.13, pp.115–120, Jan. (2005).

[9] H. Murakami, N. Uchida, R. Inoue, S. Kim, T. Kiwa, and M. Tonouchi, "Laser terahertz emission microscope," *Proc. IEEE* Vol.95, No.8, pp. 1646-1657 Aug. (2007).

[10] R. Inoue, N. Uchida, and M. Tonouchi, "Scanning Probe Laser Terahertz Emission Microscopy system," *Jpn. J. Appl. Phys.* Vol.45, No.31, pp. L824–L826, Oct. (2006).

[11] D. A. Fletcher, K. B. Crozier, K. W. Guarini, S. C. Minne, G. S. Kino, C. F. Quate, and K. E. Goodson, "Microfabricated Silicon Solid Immersion Lens", *Journal of Microelectromechanical System*, Vol.10, pp. 450–459, Sep. (2001).

[12] S. Kim, H. Murakami, and M. Tonouchi, "Transmission-type Laser THz Emission Microscope using a Solid Immersion Lens", *Journal of Selected Topics in Quantum Electronics*, in press.